INSTITUTE OF PHYSICS PUBLISHING JOURNAL OF PHYSICS D: APPLIED PHYSICS

J. Phys. D: Appl. Phys. **36** (2003) 1075–1083 PII: S0022-3727(03)58159-1

# Consequences of unburned hydrocarbons on microstreamer dynamics and chemistry during plasma remediation of $NO_x$ using dielectric barrier discharges

**Rajesh Dorai**[1,3] **and Mark J Kushner**[2,4]

[1] Department of Chemical and Biomolecular Engineering, University of Illinois, 1406, W. Green St., Urbana, IL 61801, USA
[2] Department of Electrical and Computer Engineering, University of Illinois, 1406, W. Green St., Urbana, IL 61801, USA

E-mail: rajesh.dorai@vsea.com and mjk@uiuc.edu

Received 10 January 2003
Published 16 April 2003
Online at stacks.iop.org/JPhysD/36/1075

**Abstract**
Atmospheric pressure plasmas, and dielectric barrier discharges (DBDs) in particular, are being investigated for their use in the remediation of nitrogen oxides ($NO_x$) from automotive exhausts. In their normal mode of operation, DBDs consist of a large density of short-lived filamentary microdischarges. Localized energy deposition results in spatially nonuniform gas temperatures and species densities which initiate advective and diffusive transport. Diesel exhausts, one of the major sources of $NO_x$, typically contain unburned hydrocarbons (UHCs) which significantly influence the $NO_x$ chemistry during plasma remediation. In this paper, we discuss results from a computational investigation of the consequences of UHC chemistry on radial transport dynamics and remediation of $NO_x$. In the presence of UHCs, radicals such as O and OH are dominantly consumed in the microstreamer region and their transport to larger radii is reduced. As a result, the conversion of NO to $NO_2$ is mainly restricted to the core of the microstreamer.

## 1. Introduction

Atmospheric pressure plasmas, and dielectric barrier discharges (DBDs) in particular, are being investigated for the remediation of nitrogen oxides from diesel exhausts [1–9]. (The dominant nitrogen oxides, NO and $NO_2$ are collectively referred to as $NO_x$.) During the operation of DBDs, a given volume of the gas is repetitively processed by an array of filamentary microdischarges [10, 11]. These microstreamers, typically 10s–100s of $\mu$m in diameter, occur with densities of 10s–100s $cm^{-2}$ and last a few 100s of ns. The microstreamers are regions of localized energy deposition with high densities of electrons, ions, radicals and excited species. As the remediation of $NO_x$ is initiated by the radicals produced in the microstreamers, their dynamics and kinetics have a significant influence on the efficiencies of the removal process.

Several experimental [12–14] and modelling [11, 15–21] investigations have targeted the dynamics of microstreamers in DBDs. For example, in emission spectroscopy studies of atmospheric pressure plasmas in $N_2$ by Gherardi *et al* [13], the discharges were found to transition from a glow to filamentary mode as the power deposition was increased. The axial propagation of the microstreamers results from electron avalanche in the large electric fields produced in the space-charge-dominated head of the streamer [19]. The time required

[3] Present address: Varian Semiconductor, 35, Dory Road, Gloucester, MA 01930, USA.
[4] Author to whom correspondence should be addressed.

  

for microstreamers to bridge the electrode gap is a few ns. At times later than 10s of ns, transport is dominantly in the radial direction as axial properties are fairly uniform. Since the dynamics and chemistry of interest to $NO_x$ remediation typically occur on timescales of 100s ns–ms, radial transport largely determines the process efficiency.

Unburned hydrocarbons (UHCs), often present in diesel exhausts, significantly influence $NO_x$ chemistry during plasma remediation by oxidizing NO, the major form of $NO_x$, into $NO_2$ [4, 5]. Although the source of the oxygen in this process is $O_2$ or $H_2O$, the formation of oxygen containing hydrocarbon radicals speeds the NO oxidation process. Niessen *et al* [4] used ethene ($C_2H_4$) as a model UHC and showed that the W-value (energy required to remove one molecule) for NO improved from 60 eV without $C_2H_4$ to 10 eV with 2000 ppm of $C_2H_4$. In experiments by Khacef *et al* [5], NO removal improved from 50% at 90 J l$^{-1}$ in the absence of propene ($C_3H_6$) to 90% when adding 500 ppm $C_3H_6$, with most of the NO being converted to $NO_2$.

In this paper, we report on a computational investigation of the consequences of radial dynamics of microdischarges on $NO_x$ remediation while including the plasma chemistry of UHCs. Results from a one-dimensional plasma chemistry and hydrodynamics model show that UHCs, in this case propene ($C_3H_6$), consume radicals such as O and OH which are dominantly produced in the microstreamer region and thus limit their transport to outer radii. As a result, the removal of NO is mainly restricted to the core of the microstreamer. A description of the model is given in section 2. A discussion of the consequences of reactions between UHCs and $NO_x$, and transport on remediation is in section 3. Concluding remarks are in section 4.

## 2. Description of the model

The model developed for this study is based on that described in [21]. For computational purposes, the DBD is represented as a uniform array of identically radially symmetric microdischarges. The model itself addresses only a single radially symmetric microdischarge whose properties are replicated for purposes of computing reactor averaged properties such as energy deposition. The modelled microdischarge and its surrounding volume are computationally discretized using cylindrical coordinates with variable mesh spacing. Typically, 50–100 radial points are used with spacings of a micron at the centre of the microstreamer to 10s of microns at the periphery. Reflective boundary conditions are enforced at the periphery. The width of the computational domain of the single modelled microdischarge defines the spacing of the conceptual array of microdischarges. The width of the domain is chosen large enough, typically a few mm, that hydrodynamic waves or acoustic disturbances are essentially damped before reaching the boundary and so preventing artificial reflections from 'neighbouring' microdischarges. In reality, the spacings of microdischarges are likely considerably less than a few mm. However since the microdischarges are randomly generated during the ramp up of the voltage pulse, their dynamics are isolated in time. As such, in most cases adjacent microdischarges most likely do not frequently interact.

The model is composed of a circuit module for the discharge, a solution of Boltzmann's equation for the electron energy distribution, a plasma chemistry module and a transport module. From a circuit viewpoint, the discharge is represented by a parallel set of resistors, each accounting for a computational element of a microdischarge and its surrounding volume. The circuit module provides the $E/N$ (electric field/gas number density), which is used in the calculation of the electron temperature,

$$\frac{\partial}{\partial t}\left(\frac{3}{2}n_e k_B T_e\right) = \vec{j}\cdot\vec{E} - \sum_i \frac{3}{2}n_e \nu_{mi}\left(\frac{2m_e}{M_i}\right)k_B(T_e - T_i) + \sum_l n_e k_l N_l \Delta\varepsilon_l, \quad (1)$$

$n_e$ is the electron density, $T_e$ is the electron temperature, $\vec{j}$ and $\vec{E}$ are the current density and the electric field in the axial direction in the discharge, and $\nu_{mi}$ is the electron momentum transfer collision frequency with species $i$. $m_e$ is the electron mass, $k_B$ is the Boltzmann's constant and $M_i$ and $T_i$ are the mass and temperature of species $i$. For the $l$th electron impact process, $k_l$ is the reaction rate coefficient, $N_l$ is the density of the gas phase collision partner and $\Delta\varepsilon_l$ is the change in the electron energy. Rate coefficients for electron impact reactions are obtained by solving the two-term spherical harmonic expansion of Boltzmann's equation for the electron energy distribution, parametrizing them for several values of $E/N$ and creating a lookup table interpolated using the local electron temperature [22]. The plasma chemistry module provides the local rates of change of species densities based on chemical kinetics and electron impact processes. The changes in species densities as a result of motion between the mesh points are addressed in the transport module.

The equations solved in the transport module are

$$\frac{\partial\rho}{\partial t} = \nabla\cdot(\rho\vec{v}), \quad (2)$$

$$\frac{\partial(\rho\vec{v})}{\partial t} = -\nabla P - \nabla\cdot(\rho\vec{v}\vec{v}) - \nabla\cdot\bar{\bar{\tau}}, \quad (3)$$

$$\frac{\partial(c_p\rho T)}{\partial t} = \vec{j}\cdot\vec{E} - \sum_i\left(\frac{dN_i}{dt}\right)\cdot\Delta H_i + \nabla\cdot\kappa\nabla T - \nabla\cdot(c_p\rho T\vec{v}) - P(\nabla\cdot\vec{v}) + 2\mu(\nabla\cdot\vec{v})^2, \quad (4)$$

where $\rho$ is the total mass density, $\vec{v}$ is the species average advective velocity, $P$ is the total thermodynamic pressure (assuming ideal gas behaviour) and $\bar{\bar{\tau}}$ is the viscosity tensor. $c_p$, $T$, $\kappa$ and $\mu$ are the heat capacity, average gas temperature, thermal conductivity and viscosity. $N_i$ and $H_i$ are the density and enthalpy of species $i$. In equation (4) for energy density, the terms are for Joule heating, enthalpy of reactions, thermal conduction, convection, compressible pressure heating, and viscous dissipation.

The densities of individual species are obtained from separate continuity equations,

$$\frac{\partial N_i}{\partial t} = -\nabla\cdot\left(N_i\vec{v} - \rho D_i\nabla\left(\frac{N_i}{\rho}\right)\right) + W_i, \quad (5)$$

where $D_i$ is the diffusion coefficient and $W_i$ is the source function due to electron impact and heavy particle reactions for

species $i$. Spatially dependent time derivatives are constructed using conservative finite difference donor cell techniques on a staggered mesh. $\rho$, $N_i$ and $T$ are solved for at cell vertices whereas $\rho\vec{v}$ is obtained at cell boundaries. The resulting ordinary differential equations are integrated in time using VODE [23]. We monitor the densities to determine when advective transport has dissipated and, at that point, set $\vec{v} = 0$ and continue the calculation using only diffusion. This greatly speeds the calculation while sacrificing only the resolution of small amplitude acoustic waves. To capture the features of repetitive pulses, the model is run for a series of current pulses and afterglow periods.

## 3. Consequences of UHCs on the dynamics of plasma remediation of $NO_x$

The base case conditions are $N_2/O_2/H_2O = 86/8/6$ with 500 ppm NO (1 atm, 453 K), electrode separation of 0.3 cm, gas residence time of $10^{-2}$ s, and a pulse repetition frequency of 300 Hz. A potential of 10 kV is applied across the gap. This gas mixture was chosen as, when including UHCs, a surrogate for the exhaust of on-road diesel engines. The computational area is 1 cm × 1 cm and the initial streamer radius is 10 $\mu$m. We acknowledge that the spatially averaged densities of microstreamers are considerably larger. The isolated microstreamer and the large disparity in the size of the initial streamer and total area were deliberately chosen to minimize edge effects (e.g. reflection of acoustic waves). The energy deposition in the streamer region for the base case is 170 J l$^{-1}$ for a single pulse. To put this value in perspective, the volume averaged energy deposition for a DBD operating at 1 kHz with an area density of microstreamers of 100 cm$^{-2}$ and residence time of 0.2 s is ≈10 J l$^{-1}$. The model hydrocarbon is $C_3H_6$, having a density of 2000 ppm in the base case with UHCs. Since the reaction mechanisms for $NO_x$ remediation with and without UHCs have been previously discussed [24, 25], we will focus on only those reactions of direct interest to this study.

The dominant pathways for reactions of $NO_x$ and UHCs are shown in figure 1. Briefly, the plasma remediation of $NO_x$ is initiated by O, OH and N produced by electron impact dissociation of the feedstock gases. Since energy deposition is mainly restricted to the streamer region, these radicals are dominantly produced close to the axis. N is primarily

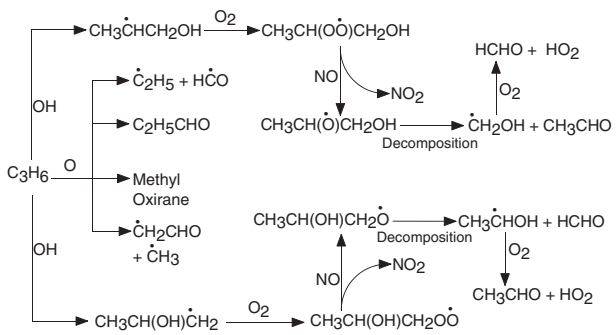


**Figure 1.** Reaction mechanism for $NO_x$ with $C_3H_6$.

consumed by reaction with NO to form $N_2$,

$$N + NO \rightarrow N_2 + O,$$
$$k = 3.4 \times 10^{-11} \exp\left(-\frac{24}{T}\right) \text{ cm}^3\text{ s}^{-1},$$
$$k_{298} = 3.2 \times 10^{-11} \text{ cm}^3\text{ s}^{-1} \text{ [26]}, \quad (6)$$

where $k$ is the temperature dependent rate coefficient and $k_{298}$ is its value at room temperature. O is dominantly consumed by reactions with $O_2$ and $C_3H_6$,

$$O + O_2 + M \rightarrow O_3 + M,$$
$$k = 3.4 \times 10^{-34} \left(\frac{T}{298}\right)^{-1.2} \text{ cm}^6\text{ s}^{-1} \text{ [26]}, \quad (7)$$

$$O + C_3H_6 \rightarrow \text{Methyl Oxirane},$$
$$k = 1.2 \times 10^{-12} \text{ cm}^3\text{ s}^{-1} \text{ [27]}, \quad (8)$$

$$O + C_3H_6 \rightarrow C_2H_5CHO,$$
$$k = 1.2 \times 10^{-12} \text{ cm}^3\text{ s}^{-1} \text{ [27]}, \quad (9)$$

$$O + C_3H_6 \rightarrow CH_2CHO + CH_3,$$
$$k = 0.8 \times 10^{-12} \text{ cm}^3\text{ s}^{-1} \text{ [27]}, \quad (10)$$

$$O + C_3H_6 \rightarrow C_2H_5 + HCO,$$
$$k = 0.8 \times 10^{-12} \text{ cm}^3\text{ s}^{-1} \text{ [27]}, \quad (11)$$

where $M$ is any third body. OH is principally consumed by reactions with NO and $C_3H_6$ to form $HNO_2$ and $C_3H_6OH$,

$$OH + NO + M \rightarrow HNO_2 + M,$$
$$k = 8.6 \times 10^{-31} \left(\frac{T}{298}\right)^{-2.5} \exp\left(\frac{34}{T}\right) \text{ cm}^6\text{ s}^{-1},$$
$$k_{298} = 9.7 \times 10^{-31} \text{ cm}^6\text{ s}^{-1} \text{ [28]}, \quad (12)$$

$$OH + C_3H_6 \rightarrow C_3H_6OH,$$
$$k = 4.9 \times 10^{-12} \exp\left(\frac{504}{T}\right) \text{ cm}^3\text{ s}^{-1},$$
$$k_{298} = 2.6 \times 10^{-11} \text{ cm}^3\text{ s}^{-1} \text{ [27]}. \quad (13)$$

Further reactions of $C_3H_6OH$ with $O_2$ result in the formation of $C_3H_6(OO)OH$ ($\beta$-hydroxy alkyl peroxy radicals or $\beta$HAPs) which react with NO to produce $NO_2$ and $C_3H_6(O)OH$ ($\beta$-hydroxy alkoxy radicals or $\beta$HAs),

$$C_3H_6OH + O_2 \rightarrow C_3H_6(OO)OH,$$
$$k = 1.6 \times 10^{-11} \text{ cm}^3\text{ s}^{-1} \text{ [27]}, \quad (14)$$

$$NO + C_3H_6(OO)OH \rightarrow NO_2 + C_3H_6(O)OH,$$
$$k = 5.4 \times 10^{-12} \exp\left(\frac{360}{T}\right) \text{ cm}^3\text{ s}^{-1},$$
$$k_{298} = 1.8 \times 10^{-11} \text{ cm}^3\text{ s}^{-1} \text{ [27]}. \quad (15)$$

The electron density $n_e$ for the base case is shown in figure 2. During the current pulse which lasts ≈70 ns, electron avalanche in the streamer occurs through electron impact ionization of $N_2$, $O_2$ and $H_2O$ and results in the production of N, O and OH radicals. The peak value of $T_e$ on-axis is 3.1 eV and the peak value of $n_e$ is $3.7 \times 10^{13}$ cm$^{-3}$. For these conditions, the electron temperature is primarily determined by

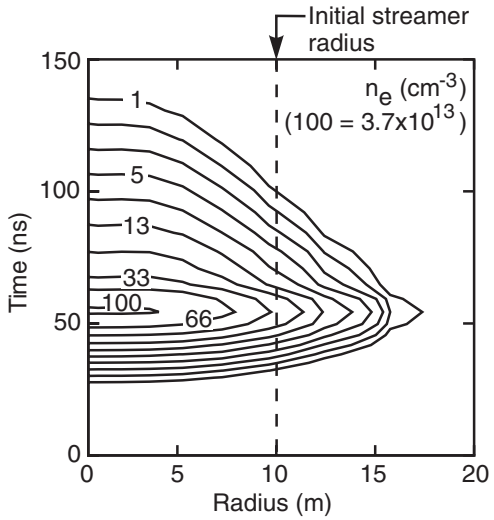


**Figure 2.** Electron density $n_e$ as a function of radius and time. Conditions are $N_2/O_2/H_2O = 86/8/6$ with 500 ppm NO (1 atm, 453 K), gas residence time of $10^{-2}$ s, 300 Hz, streamer-volume averaged energy deposition of 170 J $l^{-1}$.

$E/N$. At any given time during the current pulse, the value of $E/N$ remains nearly the same as a function of radius and so $T_e$ is fairly uniform. Following the current pulse, electrons are rapidly lost to $O_2$ and $H_2O$ by attachment and as a result their diffusion to regions far beyond the streamer is limited. Since the densities of the dominant background gases do not significantly change after any given pulse, the electron temperature and electron densities do not significantly differ from pulse to pulse.

The gas temperature, mass flux and the total gas density during and following the current pulse are shown in figure 3. Following Joule and enthalpy heating, the gas temperature rises by ≈120 K producing a pressure gradient which initiates advection radially outward. The advective wave results in the movement of the hot mass from the core producing significantly increased temperatures at radii distinctly outside of the streamer. Following the current pulse, the temperature decreases by expansion cooling and thermal conduction, while the peak in the mass flux moves radially outward. Once the core temperature decreases sufficiently, the pressure gradient reverses resulting in an influx of mass back into the streamer region. With time, the advective wave widens and flattens as a result of the opposing forces of viscosity, and pressure and thermal gradients. Advection at longer times is restricted to small acoustic waves, which, due to their small amplitude, do not significantly contribute to changes in species densities.

The densities of O atoms with and without 2000 ppm of $C_3H_6$ are shown in figure 4. During the current pulse, O atoms are dominantly produced in the streamer region by electron impact dissociation of $O_2$. Most of the O is consumed by reactions with $O_2$ to form $O_3$ (equation (7)). The production of O atoms outside of the microstreamer during and after the current pulse (a few 100s of ns) is mainly due to the ambipolar diffusion of electrons which produce O by the dissociation of $O_2$. Owing to their high reactivity, O atoms are quickly consumed (10s of $\mu$s) and hence do not accumulate pulse to pulse. Since the density of $O_2$, its primary precursor and consumer, does not significantly change from pulse to pulse,

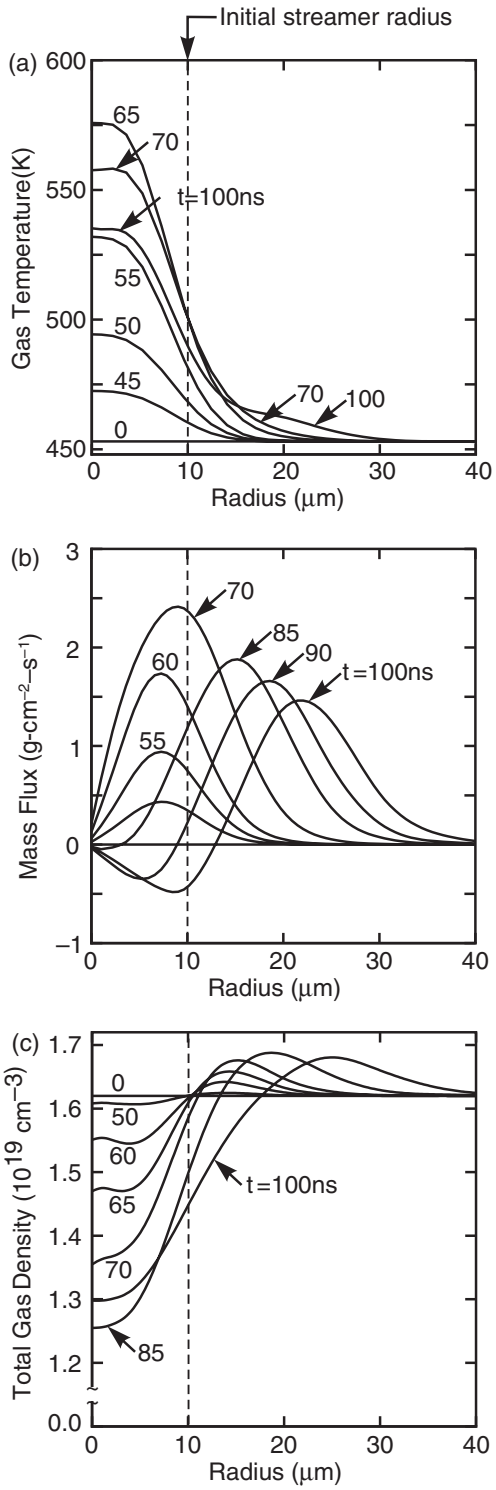


**Figure 3.** Microstreamer characteristics during the initial 100 ns. The current pulse lasts ≈70 ns. Localized energy deposition initiates radial advection. Following the current pulse, the temperature decreases by cooling and thermal conduction, and pressure gradients reverse.

O atom densities are not significantly different for the first and the last pulse.

The initial production of O atoms, primarily by electron impact dissociation of $O_2$, is not significantly influenced by $C_3H_6$ and so does not differ between the base cases with

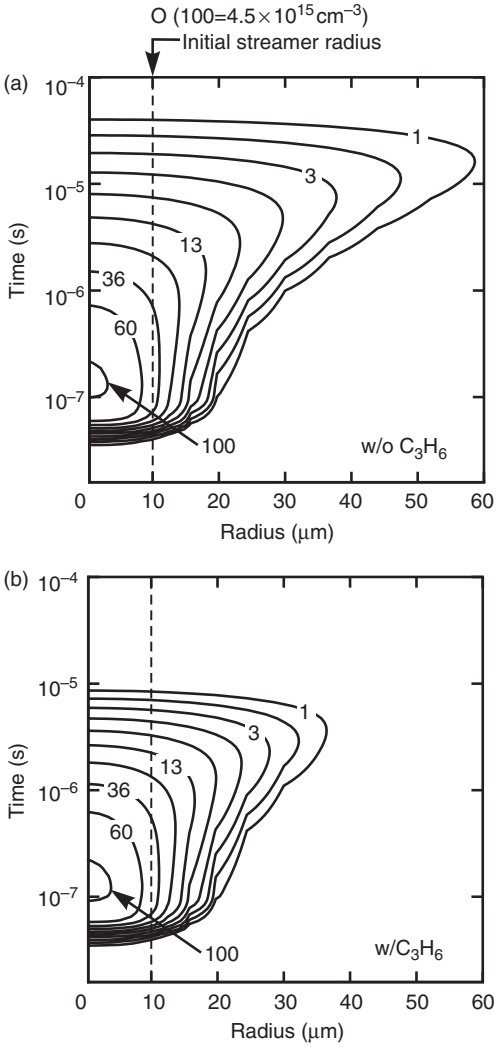


**Figure 4.** Densities of O (*a*) without $C_3H_6$, (*b*) with $C_3H_6$. Conditions are as in figure 2. O atoms are more rapidly consumed with $C_3H_6$ and hence their diffusion to larger radii is limited.

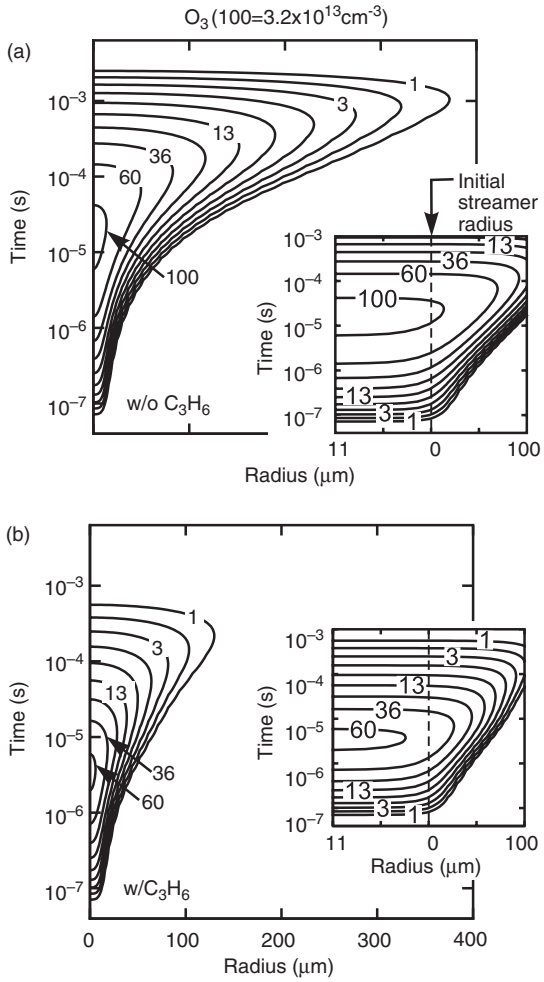


**Figure 5.** Densities of $O_3$ (*a*) without $C_3H_6$, (*b*) with $C_3H_6$. Due to the preferential consumption of O by $C_3H_6$, $O_3$ production is limited and as a result, diffusion to larger radii is restricted. Conditions are as in figure 2.

and without UHCs. At longer times (greater than many $\mu$s), O atoms are additionally consumed by reactions with $C_3H_6$ (equations (8)–(11)) and hence their densities are smaller compared to the case without UHCs. As a result, the diffusion of O beyond the microstreamer is more limited.

Since the rates for consumption of O atoms by reactions with $C_3H_6$ are larger than those with $O_2$ (equation (7)), O atoms are preferentially depleted by $C_3H_6$. Due to the decreased availability of O for reactions with $O_2$, the densities of $O_3$ are smaller compared to the case without $C_3H_6$, as shown in figure 5. Subsequently, diffusion of $O_3$ to regions outside of the microstreamer is more restricted with $C_3H_6$. $O_3$ is dominantly consumed by reactions with NO to form $NO_2$,

$$\mathrm{NO} + \mathrm{O_3} \rightarrow \mathrm{NO_2} + \mathrm{O_2},$$
$$k = 4.3 \times 10^{-12} \exp\left(-\frac{1598}{T}\right) \mathrm{cm^3\,s^{-1}},$$
$$k_{298} = 2.1 \times 10^{-14}\,\mathrm{cm^3\,s^{-1}}\ [27]. \qquad (16)$$

Since NO is abundant both within and outside the streamer region, most of the $O_3$ is consumed and does not accumulate pulse to pulse.

The densities of OH with and without $C_3H_6$ are shown in figure 6. Initially ($t < 100$ ns), OH is produced in the streamer by the electron impact dissociation of $H_2O$. At later times and in the absence of $C_3H_6$, OH is depleted in the streamer by reactions with NO to form $HNO_2$ (equation (12)) and by diffusion to outer regions. With UHCs, OH is more rapidly consumed by reactions with $C_3H_6$, to form $C_3H_6OH$ (equation (13)) and, as a result, diffusion of OH far beyond the streamer is not as pronounced as without $C_3H_6$. Due to its high reactivity, OH does not accumulate pulse to pulse.

Electron impact dissociation of $H_2O$ also produces H, most of which reacts with $O_2$ to form $HO_2$,

$$\mathrm{H} + \mathrm{O_2} + \mathrm{M} \rightarrow \mathrm{HO_2} + \mathrm{M},$$
$$k = 1.8 \times 10^{-32} \left(\frac{T}{298}\right)^{-0.8} \mathrm{cm^6\,s^{-1}}\ [29]. \qquad (17)$$

The densities of $HO_2$ with and without $C_3H_6$ are shown in figure 7. With $C_3H_6$, more $HO_2$ is produced by reactions of

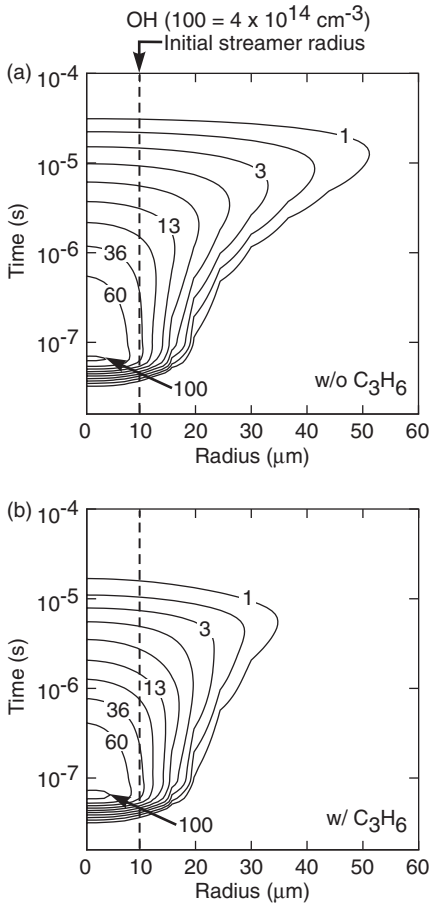


**Figure 6.** Densities of OH (*a*) without $C_3H_6$, (*b*) with $C_3H_6$. Conditions are as in figure 2. OH radicals are more rapidly consumed with $C_3H_6$ and hence their diffusion to larger radii is restricted.

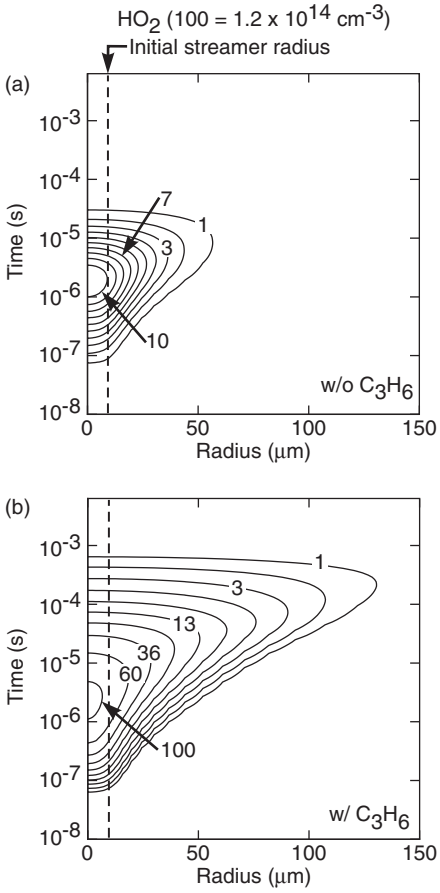


**Figure 7.** Densities of $HO_2$ (*a*) without $C_3H_6$, (*b*) with $C_3H_6$. Due to the additional production of $HO_2$ by $C_3H_6$ initiated reactions, the densities of $HO_2$ are larger with $C_3H_6$.

$O_2$ with the products of $\beta$HA radical decomposition,

$$C_3H_6(O)OH \rightarrow CH_3CHOH + HCHO,$$
$$k = 7.9 \times 10^{13} \exp\left(-\frac{10\,517}{T}\right) \text{ s}^{-1},$$
$$k_{298} = 3.7 \times 10^{-2} \text{ s}^{-1} \text{ [26]}, \tag{18}$$

$$CH_3CHOH + O_2 \rightarrow CH_3CHO + HO_2,$$
$$k = 1.9 \times 10^{-11} \text{ cm}^3 \text{ s}^{-1} \text{ [30]} \tag{19}$$

and so the densities of $HO_2$ are sustained for longer times. Depletion of $HO_2$ occurs by diffusion to outer radii and by reaction with NO to produce $NO_2$,

$$NO + HO_2 \rightarrow NO_2 + OH,$$
$$k = 3.5 \times 10^{-12} \exp\left(\frac{240}{T}\right) \text{ cm}^3 \text{ s}^{-1},$$
$$k_{298} = 7.8 \times 10^{-12} \text{ cm}^3 \text{ s}^{-1} \text{ [27]}. \tag{20}$$

The densities of NO for the cases with and without $C_3H_6$ are shown in figure 8. Rarefaction of the core from advection results in the depletion of NO from the streamer region and accumulation of NO outside. At later times, reversal of the pressure gradient and back diffusion refills NO in the microstreamer. This refilling of the core from the large reservoir of NO around the streamer results in only small fractional changes in NO pulse to pulse. Remediation is ultimately produced by the combined effects of 100s of such microstreamers per unit area. With $C_3H_6$, more NO is consumed by reactions with $\beta$HAPs (equation (15)) and $HO_2$ (equation (20)). As a result the density of NO at any given time and radial location is smaller than that without $C_3H_6$. Correspondingly, it takes a longer time to repopulate NO in the streamer by diffusion from outside.

The densities of $NO_2$ with and without $C_3H_6$ are shown in figure 9 for the first and third of a series of pulses. More $NO_2$ is produced with $C_3H_6$ by the reactions of $\beta$HAP radicals with NO (equation (15)). Without $C_3H_6$, $NO_2$ is mainly formed by the reactions of NO with $O_3$ and $HO_2$ (equations (16) and (20)) at timescales of a few to 10s of $\mu$s. Due to the smaller reactivity of $NO_2$ compared to NO, the density of $NO_2$ accumulates from pulse to pulse as shown by the increase in $NO_2$ from the first to the third pulse in figure 9. The accumulation is more pronounced with $C_3H_6$ due to the larger production of $NO_2$.

The densities of $C_3H_6$ and $\beta$HAPs are shown in figure 10. Initial radial advection depletes $C_3H_6$ from the streamer and results in a peak in its density at the streamer edge. Refilling of the core at later times partly restores its density. As with NO, although $C_3H_6$ is depleted in the streamer by reactions with O

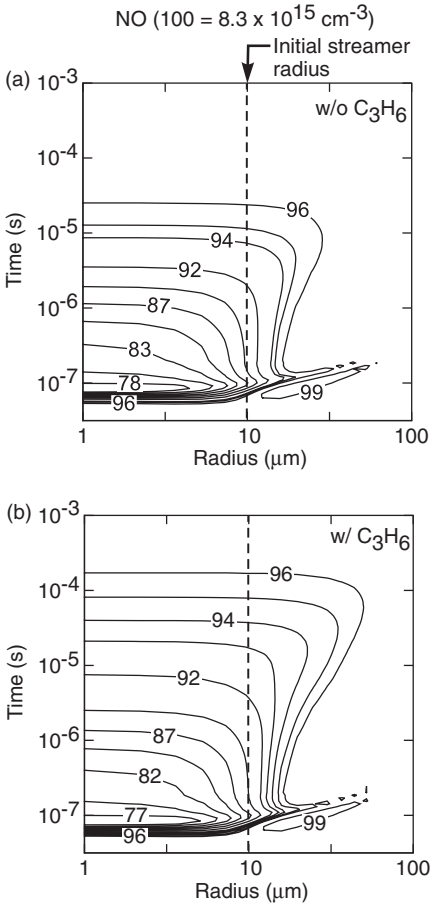


**Figure 8.** Densities of NO (*a*) without $C_3H_6$, (*b*) with $C_3H_6$. Conditions are as in figure 2. With $C_3H_6$, more NO is consumed in the streamer by reactions with $\beta$HAP radicals and as a result NO densities are smaller at any given time.

and OH, diffusion from the large volume of $C_3H_6$ outside the streamer compensates for the losses. Consumption of $C_3H_6$ by OH produces $\beta$HAP radicals (equations (13) and (14)), which further react with NO to produce $NO_2$ (equation (15)). With time, $\beta$HAPs in the streamer are depleted by reactions with NO and by diffusion to outer radii.

Although most of the NO that is consumed is by conversion to $NO_2$, NO is also lost by reactions with OH to form $HNO_2$ (equation (12)). The densities of $HNO_2$ with and without UHCs are shown in figure 11. With UHCs, OH is preferentially consumed by reactions with $C_3H_6$ and so less is available for reactions with NO. As a result, the initial production of $HNO_2$ is smaller. At later times, larger densities of $HNO_2$ are sustained with $C_3H_6$ by the reaction of $HO_2$ with $NO_2$,

$$HO_2 + NO_2 \rightarrow HNO_2 + O_2,$$
$$k = 1.2 \times 10^{-13}\ \mathrm{cm^3\ s^{-1}}\ [26]. \qquad (21)$$

Since the densities of $HO_2$ and $NO_2$ are larger and are sustained for longer periods with $C_3H_6$ (see figures 7 and 10), more $HNO_2$ is produced at longer times.

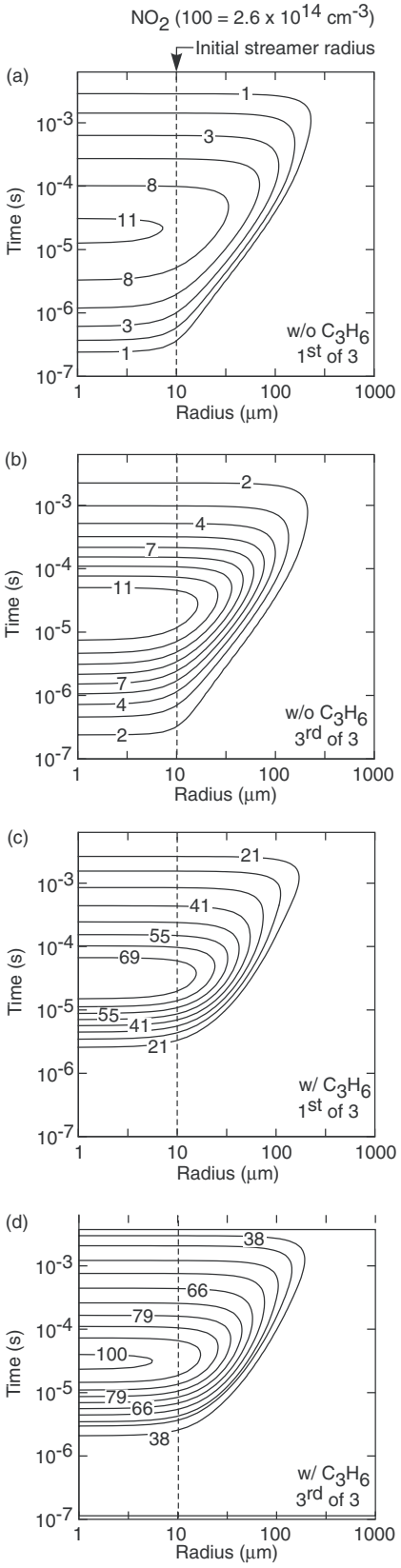


**Figure 9.** Densities of $NO_2$ for the first and third of a series of pulses. (*a*) First and (*b*) third pulse without $C_3H_6$. (*c*) First and (*d*) third with $C_3H_6$. Conditions are as in figure 2. Due to the increased conversion of NO to $NO_2$ with $C_3H_6$, $NO_2$ densities are larger.

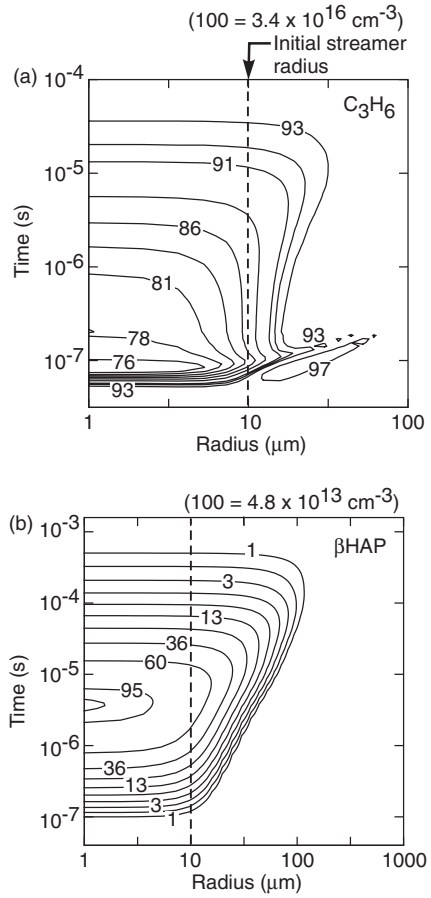


**Figure 10.** Species density (*a*) $C_3H_6$, (*b*) $\beta$HAPs. Radial advection results in transport of $C_3H_6$ outside of the streamer. $C_3H_6$ is consumed by reactions with O and OH.

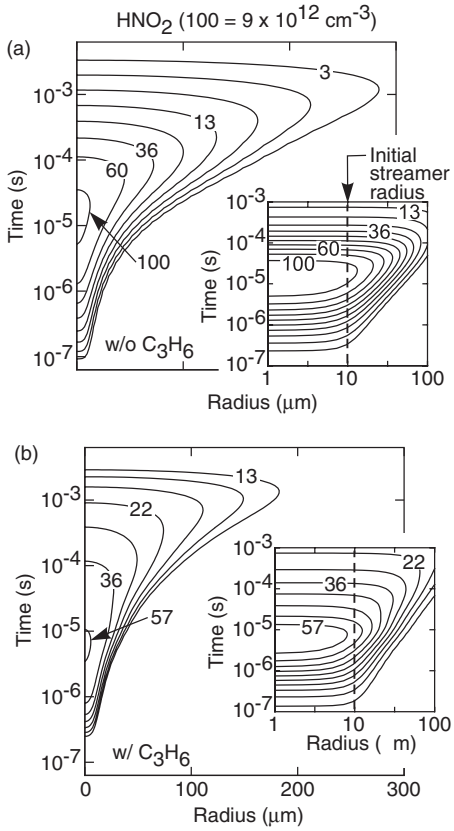


**Figure 11.** Densities of $HNO_2$ (*a*) without $C_3H_6$, (*b*) with $C_3H_6$. For $t < 10$ s of $\mu$s, $HNO_2$ is primarily produced by the reactions of OH with NO. Due to the increased consumption of OH with $C_3H_6$, less $HNO_2$ is initially produced. The larger densities of $HNO_2$ at longer times with $C_3H_6$ are due to the increased densities of $HO_2$ and $NO_2$ (equation (20)).

The on-axis densities of NO and $NO_2$ as a function of time and energy deposition are shown in figure 12. For $t < 100$ ns, rarefaction of the streamer region by radial advection depletes NO on the axis. Increasing energy deposition results in larger gas temperatures in the core which lead to increased rarefaction. Reversal of the pressure gradient and back diffusion refill NO in the streamer at later times. Most of the NO that is consumed is by reactions with $\beta$HAPs, $HO_2$ and $O_3$ to form $NO_2$ (equations (15), (16) and (20)). With increasing energy deposition, larger amounts of these radicals are produced and as a result, more $NO_2$ is formed. Due to the small initial radius of the streamer, depletion of NO is overshadowed by the diffusion of NO from the abundant reservoir of NO outside. At $t > 10^{-3}$ s, the density of NO is levelled by diffusion.

## 4. Concluding remarks

In the filamentary mode of operation of atmospheric pressure plasmas, energy is dominantly deposited in confined volumes resulting in localized temperature rise. This initiates advection leading to transport of species to and from the microstreamer. $C_3H_6$, representative of the UHCs typically found in diesel exhausts, reacts with the O and OH radicals produced in the streamer and limits their transport to larger radii. This process restricts the remediation of NO to the streamer region. However, with UHCs, NO conversion selectively increases in the streamer region due to the larger production of $\beta$HAPs and $HO_2$ which efficiently convert NO to $NO_2$. Since processing occurs in more confined regions with large densities of UHCs, $NO_x$ remediation is less distributed in the reactor. Therefore systems which have large gas flows and short residence times may be more sensitive to sub-volumes of gas passing through the reactor without intersecting these smaller confined regions of processing and in doing so escape treatment. Without UHCs, diffusion is more efficient at mixing treated and untreated volumes. In such cases, operating at higher repetition rates for the same average power is a preferred mode of operation to increase the likelihood that any given gas volume is treated by a microstreamer. In this regard, discharge operation strategies which maximize the area density of microdischarges will most likely produce optimum remediation. Previous work has also shown that, for a given energy deposition, it is more beneficial to treat a single volume of gas with a series of smaller energy deposition pulses compared to treating the gas with a single pulse [31]. In this regard, having a larger area density of microdischarges will also result in more energy efficient processing.

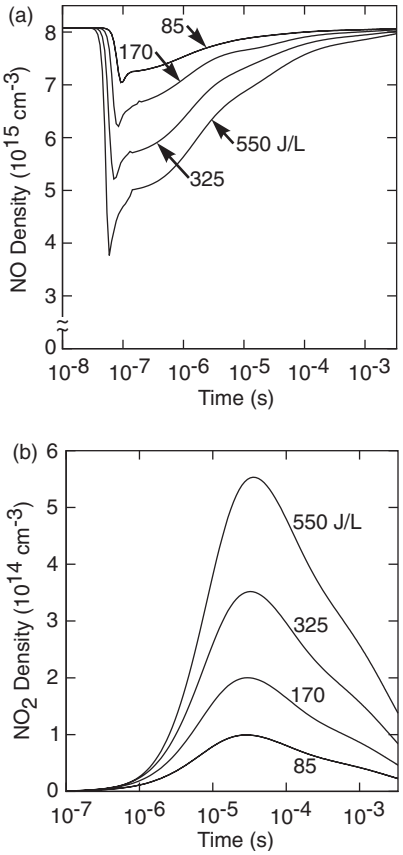


**Figure 12.** On-axis densities of NO and $NO_2$ as a function of time for energy deposition in the streamer region of 85–550 J$l^{-1}$. These values correspond to ≈6–35 J$l^{-1}$ on a time and volume averaged basis (*a*) NO, (*b*) $NO_2$. Increasing energy deposition results in larger densities of $\beta$HAPs which lead to increased conversion of NO to $NO_2$.

## Acknowledgments

This work was supported by the Ford Motor Company and the National Science Foundation (CTS99-74962).

## References

[1] Filimonova E A, Amirov R H, Kim H T and Park I H 2000 *J. Phys.* D **33** 1716
[2] Fresnet F, Baravian G, Magne L, Pasquiers S, Postel C, Puech V and Rousseau A 2002 *Plasma Sources Sci. Technol.* **11** 152
[3] McLarnon C R and Penetrante B M 1998 *SAE Tech. Paper Ser.* **982433**
[4] Niessen W, Wolf O, Schruft R and Neiger M 1998 *J. Phys.* D **31** 542
[5] Khacef A, Cormier J M and Pouvesle J M 2002 *J. Phys.* D **35** 1491
[6] Penetrante B M, Hsiao M C, Merritt B T, Vogtlin G E, Wallman P H, Neiger M, Wolf O, Hammer T and Broer S 1996 *Appl. Phys. Lett.* **68** 3719
[7] Sun W, Pashaie B, Dhali S and Honea F 1996 *J. Appl. Phys.* **79** 3438
[8] Wegst R, Neiger M, Russ H and Liu S 1999 *SAE Tech. Paper Ser.* **1999-01-3686** 1
[9] Stefanovic I, Bibinov N K, Deryugin A A, Vinogradov I P, Napartovich A P and Wiesemann K 2001 *Plasma Sources Sci. Technol.* **10** 406
[10] Pashaie B, Dhali S and Honea F 1994 *J. Phys.* D **27** 2107
[11] Pietsch G J, Braun D and Gibalov V I 1993 *Non-Thermal Plasma Techniques for Pollution Control* vol G 34, (part A) ed B M Penetrante and S E Schultheis (Berlin: Springer) p 273
[12] Falkenstein Z and Coogan J J 1997 *J. Phys.* D **30** 817
[13] Gherardi N, Gouda G, Gat E, Ricard A and Massines F 2000 *Plasma Sources Sci. Technol.* **9** 340
[14] Ohsawa A, Morrow R and Murphy A B 2000 *J. Phys.* D **33** 1487
[15] Naidis G V 1996 *J. Phys.* D **29** 779
[16] Naidis G 1997 *J. Phys.* D **30** 1214
[17] Kanzari Z, Yousfi M and Hamani A 1998 *J. Appl. Phys.* **84** 4161
[18] Kulikovsky A A 1994 *J. Phys.* D **27** 2564
[19] Kulikovsky A A 1994 *J. Phys.* D **27** 2556
[20] Vitello P A, Penetrante B M and Bardsley J N 1994 *Phys. Rev.* E **49** 5574
[21] Gentile A C and Kushner M J 1996 *J. Appl. Phys.* **79** 3877
[22] Rockwood S D 1973 *Phys. Rev.* A **8** 2348
[23] Brown P N, Hindmarsh A and Byrne G D 1998 *VODE—Variable-coefficient Ordinary Differential Equation Solver*
[24] Gentile A C and Kushner M J 1995 *J. Appl. Phys.* **78** 2074
[25] Dorai R and Kushner M J 2000 *J. Appl. Phys.* **88** 3739
[26] Mirokin Y and Mallard G 1998 *The NIST Chemical Kinetics Database*
[27] Atkinson R 1997 *J. Phys. Chem. Ref. Data* **26** 215
[28] Tsang W and Herron J T 1991 *J. Phys. Chem. Ref. Data* **20** 609
[29] Baulch D L *et al* 1994 *J. Phys. Chem. Ref. Data* **23** 847
[30] Atkinson R, Baulch D L, Cox R A, Hampson R F Jr, Kerr J A, Rossi M J and Troe J 1997 *J. Phys. Chem. Ref. Data* **26** 521
[31] Dorai R and Kushner M J 2001 *J. Phys.* D **34** 574